models produced do not replace filtration theory, although they give a good overview of the overall filtration cycle behaviour. It should be remembered that the variable ranges used in this kind of experimental work are limited by the same factors as in industrial processes and therefore these models should not be used beyond the ranges specified.

The results presented in this paper clearly and reliably demonstrate that by using factorial experimental design, the number of filtration tests required to determine the main effects of five filtration process variables could be reduced from 43 to 8 without losing a considerable amount of information. The smallest experimental design this software creates could be used to model the behaviour of the sample case. It is the user's decision how small an experimental design could be used, and it has to be reconsidered on a case -by-case basis.

The examples also show that linear regression models could be quite successfully used to describe the studied filtration process. The experimental work done during the software project showed that filtration capacities and cake moisture content were well modelled with linear models. The results for some processes, for example the cake washing, which is non-linear in nature, need to be viewed with caution. If examined processes turn out to be strongly non-linear in their behaviour, or if considerable variable interactions exist, simple linear models often fail to give satisfactory results. In these cases, more complicated models have to be created with the introduction of additional components. The most commonly applied components for this purpose are direct variable interaction terms and squared variables. The addition of these components, however, renders the models more complicated and more difficult to interpret. For non-linear responses, the experimental design from LabTop provides a good starting point for further test design.

The LabTop software shows the strength of factorial experimental design and helps create measurement data that is structured for further analysis. It also works well in establishing the overall effects of selected variables on the response and provides tools for visualization of these effects.

REFERENCES

1. Tarleton E.S. and Willmer S.A., 1997. The effects of scale and process parameters in cake filtration, *Chem. Eng. Res. Des.*, **75**(5), 497-507.
2. Herath B., Albano C., Anttila A. and Flykt B., 1992. Empirical modelling of a dewatering process using multivariate data analysis, *Filtn. & Sepn.*, **29**(1), 57-65.
3. Tarleton E.S. and Hancock D.L., 1997. Using mechatronics for the interpretation and modelling of the pressure filter cycle, *Chem. Eng. Res. Des.*, **75**(3), 298-308.
4. Box G.E.P., Hunter J.S. and Box W.G., 2005. *Statistics for Experimenters: Design, Innovation, and Discovery, 2nd Edn.*, Wiley, New Jersey.
5. Montgomery D.C., 1997. *Design and Analysis of Experiments, 4th Edn.*, Wiley, New Jersey.
6. Mayer E., 2000. Cake filtration theory and practice, *Chem. Eng. J.*, **80**(1-3), 233-236.
7. Ruslim F., Nirschl H., Stahl W. and Carvin P., 2007. Optimization of the wash liquor flow rate to improve washing of pre-deliquored filter cakes, *Chem. Eng. Sci.*, **62**(15), 3951-3961.
8. Tarleton E.S., 2008. Cake filter scale-up, simulation and data acquisition - A new approach, *J. Chin. Inst. Chem. Eng.*, **39**(2), 151-160.
9. Wakeman R.J. and Tarleton E.S., 2005. *Solid/Liquid Separation - Principles of Industrial Filtration, 1st Edn.*, Elsevier, Oxford.

ROTATIONAL PARTICLE SEPARATOR: AN EFFICIENT METHOD TO SEPARATE MICRON-SIZED DROPLETS AND PARTICLES FROM FLUIDS

J.J.H. Brouwers (j.j.h.brouwers@tue.nl), H.P. van Kemenade and J.P. Kroes
Eindhoven University of Technology, P.O. Box 513, 5600MB Eindhoven, The Netherlands.

The rotational particle separator (RPS) has a cyclone type housing within which a rotating cylinder is placed. The rotating cylinder is an assembly of a large number of axially oriented channels, e.g. small diameter pipes. Micron-sized particles entrained in the fluid flowing through the channels are centrifuged towards the walls of the channels. Here they form a layer or film of particles, material which is removed by applying pressure pulses or by flowing of the film itself. Compared to conventional cyclones the RPS is an order of magnitude smaller in size at equal separation performance, while at equal size it separates particles ten times smaller. Applications of the RPS considered are ash removal from hot flue gases in small scale combustion installations, product recovery in the stainless environment for pharmaceutical/food, oil water separation and demisting of gases. Elementary formulae for separation performance are presented and compared with measurements performed with various RPS designs.

INTRODUCTION

Many processes require the separation of micron-sized particles from a gas stream. Techniques employed to do the job are scrubbers, fabric filters, electrostatic separators, and (multi-)cyclones. There is still a drive, however, to develop new technologies: scrubbers are sizeable and fail to remove micron-sized particles, fabric filters and electrostatic precipitators are limited to dry and/or chargeable particulate matter and involve large installations, and cyclones in industrial installations that are subject to large volume flows fail to collect micron-sized particles[1]. A new development which overcomes several of the aforementioned limitations is the rotational particle separator, in short RPS[2]. The RPS has a cyclone type housing within which a rotating cylinder is placed. The rotating cylinder is an assembly of a large number of axially oriented channels. These channels provide the means to collect micron-sized particles at limited rotational speed, pressure drop and short residence time (small building volume).

In this paper we show the advantage of the RPS by comparing its performance with that of vane type separators and cyclones. These considerations are substantiated by the results of experiments. Many RPS devices have been designed and tested over the years and the lessons learned concerning flow stability, power consumption and loading/removal are discussed. An overview of the designs that have been realized is given, while the most recent design, a gas scrubber for large volume operations, is treated in more detail.

ELEMENTARY SEPARATION: VANE-TYPE SEPARATOR, CYCLONE AND RPS

We shall compare the performance of devices in which separation is the result of inertial or centrifugal forces acting on particles with different density compared to that of the fluid in which they are immersed.

The vane type separator is represented by a flow through a single bend (Figure 1). Three forces act on a particle moving along a curved trajectory with radius r and velocity v_θ: the centrifugal force F_c, a drag force F_d and a buoyancy force F_{buo}: $F_c = F_d + F_{buo}$. For particles with diameters ranging from about 0.5 to 25 µm, the fluid force can be described by Stokes flow. For smaller and larger particles Cunningham and Reynolds number corrections have to be introduced, respectively. However, at a diameter of 1 µm the effect is only about 10%, omitting it is a more conservative approach[1]. The radial migration velocity of a particle can then be described as

$$V_{TC} = \frac{(\rho_p - \rho_F) d_p^2 v_t^2}{18 \mu r} \qquad (1)$$

ρ_p and ρ_F are the densities of the particle and the carrier fluid, respectively, μ denotes the dynamic viscosity of the carrier fluid and v_t the tangential velocity. We can now turn our attention to the collection efficiency. The trajectory of a particle can be described as $dr/d\theta = rV_{TC}(r)/v_{ax}$ with the assumptions that the velocity of the fluid, v_{ax}, is uniform, there are no secondary flows and the tangential particle velocity is equal to the carrier fluid velocity, v_{ax}. Integration gives

$$r(\theta) = r(0) + \frac{(\rho_p - \rho_F) d_p^2 v_{ax}}{18 \mu} \theta \qquad (2)$$

where r and θ are the radial and angular position. With the assumption that the particles are uniformly distributed over the cross section when entering the separation device, the efficiency of the separator can be derived as

$$\varepsilon = \frac{r(\theta_{sep}) - r_i}{r_0 - r_i} = \frac{(\rho_p - \rho_f) d_p^2 v_{ax}}{18 \mu (r_0 - r_i)} \theta_{sep} \qquad (3)$$

θ_{sep} denotes the angle of the bend and r_o and r_i are the outer and inner radius. We can now determine the particle size that can be separated with 50% efficiency ($\varepsilon = 0.5$) as

$$d_{p50} = \sqrt{\frac{9 \mu d_c}{(\rho_p - \rho_F) v_{ax} \theta_{sep}}} \qquad (4)$$

with the channel height $d_c = r_o - r_i$. In practice the minimum channel height is restricted to about a millimetre. The velocity is limited by liquid entrainment and droplet break-up, typical values are below 10 m s^{-1}. For air-water under ambient pressure, this corresponds to a minimal d_{p50} value in the order of 10 µm.

The axial cyclone consists of a stationary cylindrical pipe which at the entrance contains stationary vanes or blades (Figure 2). Fluid which enters the pipe and

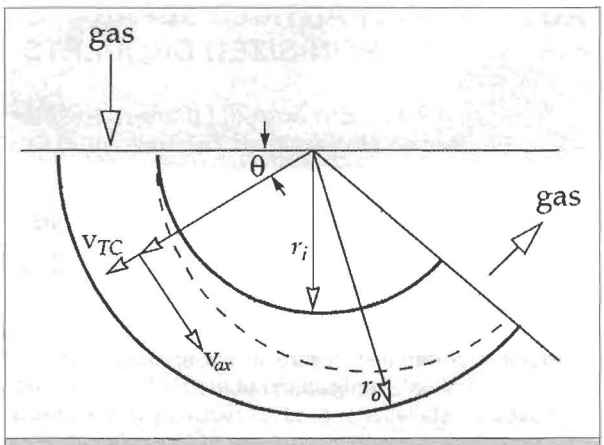

Figure 1: Vane type separator.

passes through these blades attains a swirling motion. The dispersed phase entrained in the fluid acquires this swirling motion as well. Having a density which is higher than the density of the carrier fluid, the dispersed phase will be subjected to a centrifugal force which causes it to move radially toward the cylindrical wall. It leaves the device via outlets so situated at the end of the pipe constituting the axial cyclone. Using a method analogous to the derivation of equation (4), an expression for the d_{p50} is[3]:

$$d_{p50} = \sqrt{\frac{9\mu v_{ax} R^2}{2(\rho_p - \rho_f) v_t^2 L}} \qquad (5)$$

v_t is the tangential velocity, L the length of the cyclone and R the radius. To derive this equation it is assumed that the axial velocity v_{ax} is constant over the radius.

Typical cyclones have a swirl ratio $S = v_t/v_{ax}$ of 1-2 and an L/R of ~5. The axial velocity can be higher compared to the vane type in the order of 20 m s^{-1}. The only free parameter is now the radius, i.e. to achieve a d_{p50} of 10 µm the radius has to be below 0.15 m. For higher volume flows multi-cyclones have to be used.

The inline version of the RPS is an axial cyclone within which a rotating separation element is built (Figure 3). The rotating element consists of a multitude of axially oriented channels with a diameter of about 1 to 2 mm. The separation process taking place in the channels of the RPS is similar to that in the cyclone. In this case we can derive for d_{p50}[1]:

$$d_{p50\%} = \sqrt{\frac{27\mu v_{ax} d_c R}{2(\rho_p - \rho_f) v_t^2 L}} \qquad (6)$$

We can now compare the performance of the RPS to the vane separator by looking at the ratio of d_{p50} for the same axial velocities

$$\frac{d_{p50,vane}}{d_{p50,RPS}} = \sqrt{\frac{36}{27}\frac{1}{\theta_{sep}}\frac{L}{R}S^2} \qquad (7)$$

While the separation angle is limited to about $\theta_{sep} = \pi/2$, the ratios R/L and $S = v_t/v_{ax}$ can be used for the RPS to increase performance. The d_{p50} of the cyclone compares to the d_{p50} of the RPS as

$$\frac{d_{p50,cyc}}{d_{p50,RPS}} = \sqrt{\frac{R}{3d_c}} \qquad (8)$$

Figure 4 depicts the d_{p50} under atmospheric pressure as a function of the volume flow $Q = \pi R^2$. The d_{p50} of the RPS remains constant and below 1 µm, while the cyclone d_{p50} quickly rises into the micrometre range. At equal flow and dimensions the RPS is able to separate an order of magnitude smaller particles than the axial cyclone. For equal separation performance we find the relation

$$\frac{R_{cyclone}}{R_{RPS}} = \sqrt{\frac{d_c}{3R_{cyclone}}} \qquad (9)$$

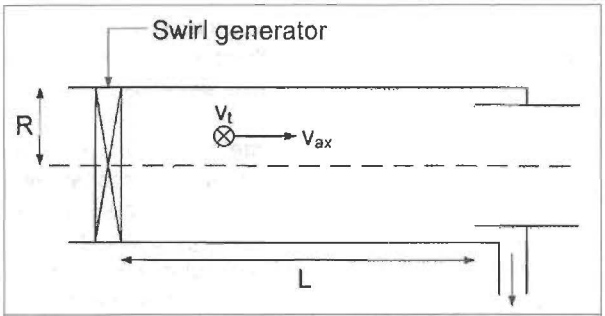

Figure 2: Schematic of axial cyclone.

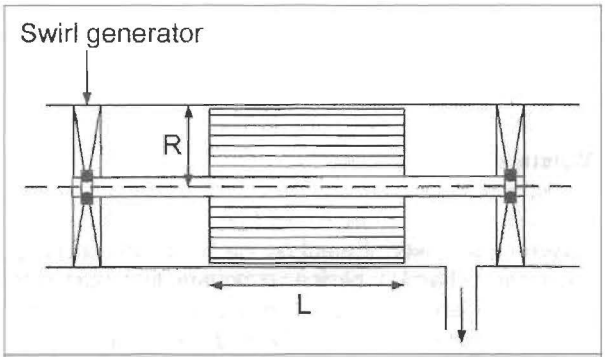

Figure 3: Schematic of axial RPS.

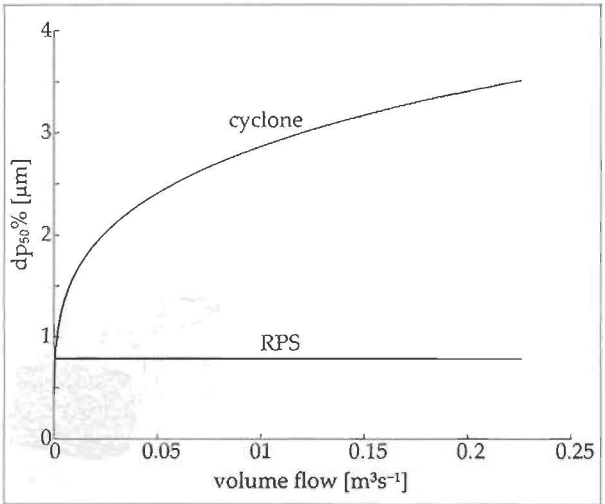

Figure 4: Diameter of water droplets in air separated by a cyclone and RPS as a function of the volume flow under atmospheric pressure.

This ratio is a measure of the difference in footprint or space between the cyclone and RPS for an equal separation performance. For the same separation performance, the size of the RPS can be an order lower compared to a cyclone.

EXPERIMENTS

Two measurement methods were used to assess the performance of the centrifugal separators: laser diffraction and impactation. Laser diffraction is based on the phenomenon that particles illuminated by a laser beam scatter light at angles that are inversely proportional to the size of the particles. Large particles scatter at small forward angles while small particles scatter light at wider angles. Mie theory is used to establish the relation between the scattered energy distribution on the detectors and the particle size distribution. In both cases the measurement setup is such that the droplet distribution of a nozzle can be measured with and without the separator in place. If the nozzle droplet distribution overlaps the separator cutoff, the separator efficiency as a function of the size can be deduced from both droplet distributions. The other apparatus used is an Anderson type cascade impactor whereby particles within a size class are collected on a specific stage of the impactor.

Moisture Separation Panel

As representative of bend-type separators, we used a moisture separation panel like that applied to the inlet of turbo machinery. Based on the fixed dimensions of the laser diffraction device, a square test duct with external dimensions of 220 mm was used to guide the air and droplets to the water droplet panels and through a Malvern MasterSizer S (Figure 5). Complying with the standard installation, a fan was installed downstream of the duct. The laser measurement is located about 300 mm downstream from the outlet of the water droplet catcher panels in order to have sufficient mixing downstream of the separator panel without encountering significant evaporation of the droplets. Adapter pieces were constructed to allow both vertical and 15° installation. Before each spray spectrum measurement was done, the setting of the fan was checked by measuring the velocity in the middle of the duct with a hot wire measuring device. Analysis of the moisture separator panels was done at 3 and 5 m s^{-1}.

A typical measurement result is depicted in Figure 6. Each datapoint represents three measurements of both the nozzle distribution and the distribution after the separator. Curve (1) is the measured droplet volume distribution without a separator in the duct. Curve (2) is measured with the separator mounted between the nozzle and the measuring spot. Curve (3) is Curve (2) scaled to Curve (1) using the measured concentration. The probability P that a particle of a certain diameter passes through the separator is found by dividing the values of Curve (3) by those of Curve (2). The efficiency is equal to the probability that a particle is caught in the separator or $\varepsilon = 1 - P$. Conventionally the cutoff diameter of a separator is characterized by the diameter d_{p50} of the particle that has a 50% probability of passing through the separator, 22 µm in the case of Figure 6.

The measured efficiencies scaled to their respective d_{p50} are presented in Figure 7. The three panel types have slightly different geometries, but all panels essentially depend on two bends for the removal of droplets. Consequently the curves overlap each other despite their difference in d_{p50}. The exception is panel type 3 at the higher velocity of 5 m s^{-1} where re-entrainment or flooding occurs, a phenomenon that is reported in literature since 1939[4]. It can be concluded that the d_{p50} is indeed a good measure to compare the performance of geometrically similar moisture panels as the efficiency distribution hardly changes.

Cyclone

The demisting stage of advanced gas-liquid scrubber vessels usually consists of a bank of axial cyclones (swirl tubes) working in parallel. We measured the efficiency of a single commercial swirl tube in the way explained in the previous section. Since the droplets

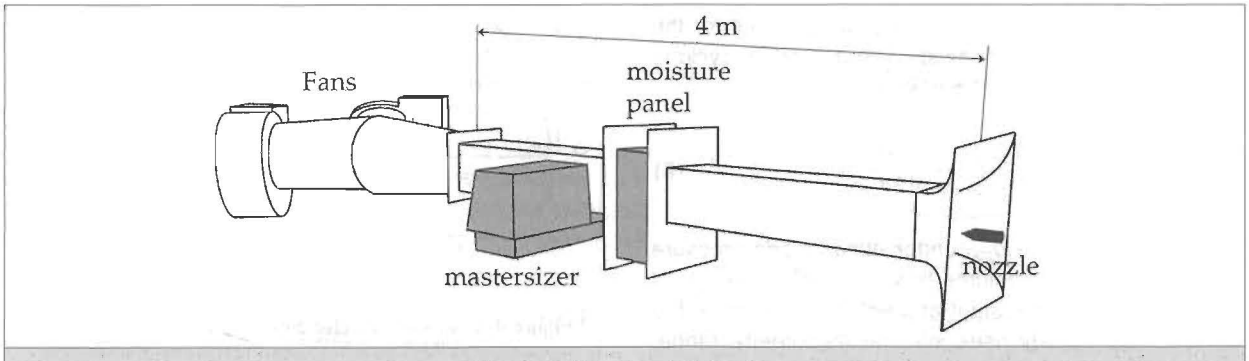

Figure 5: Experimental set-up.

leaving the cyclone are in the range 1- 10 µm, the lens of Malvern's MasterSizer S was too small so we used the Spraytec instead.

During measurements the cyclone was contained in a bigger pipe (diameter 200 mm), thereby simulating a scrubber vessel with upwards gas flow. Nozzles injected a constant amount of water into an adjustable airflow. Droplet distributions and concentrations were measured in the open outflow above this pipe. The efficiency was determined by taking a dummy cyclone (without the swirl element, i.e. vanes and body removed) as reference. Measurements were done at 11 flow rates, for which the corresponding values of d_{p50} according to equation (5) are shown in Figure 8. Figure 9 shows the combined result of all measured efficiency curves.

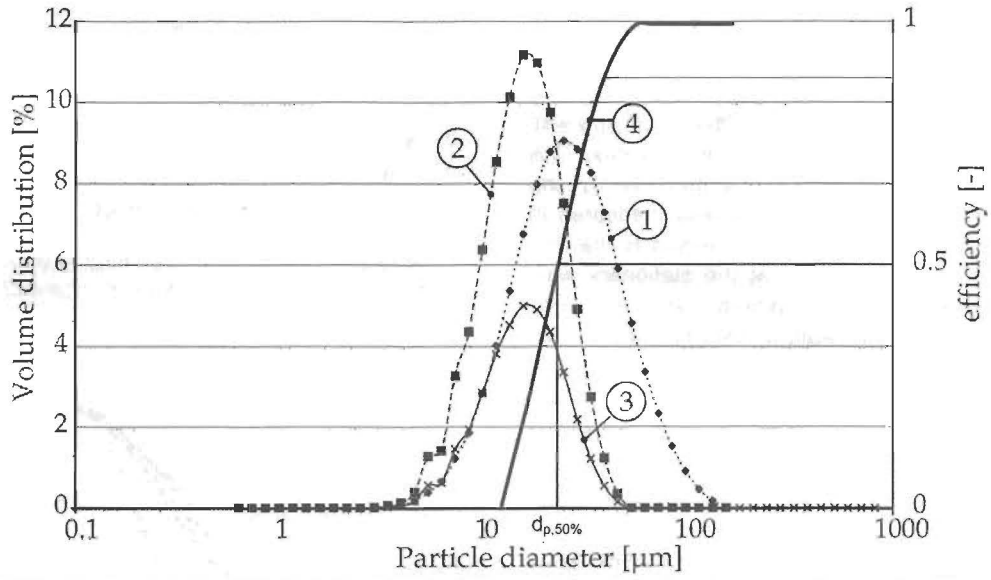

Figure 6: Typical measurement result: Curves (1) to (2) are the volume distributions measured without and with the separator present. Curve (3) is Curve (2) scaled to (1). The efficiency Curve (4) is obtained as 1-(3)/(1).

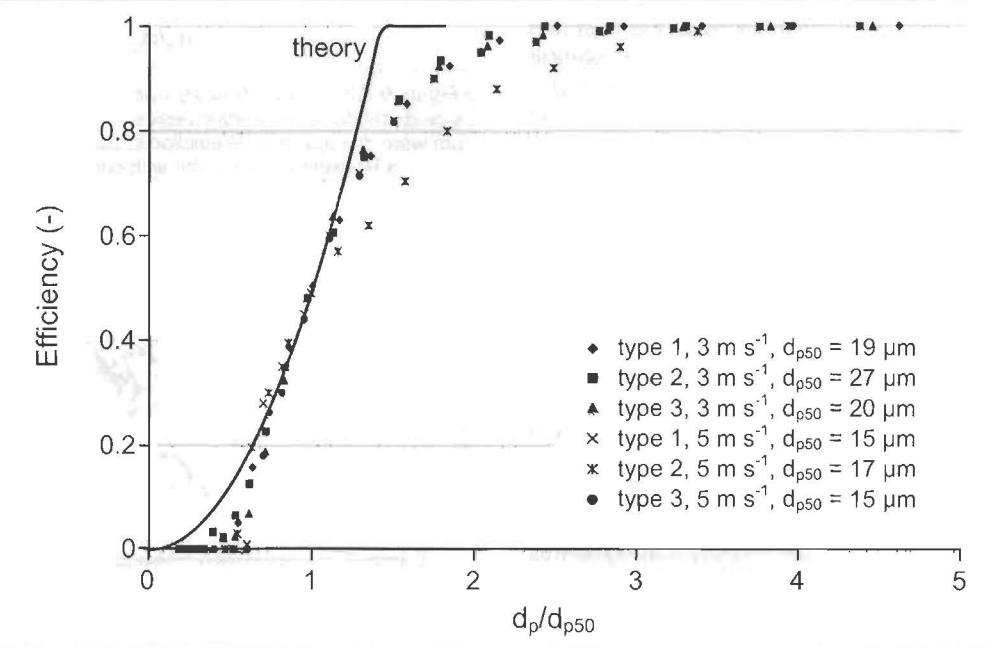

Figure 7: Measured panel efficiency.

Since all 11 curves fall virtually on one line we can conclude that d_{p50} accounts correctly for the flow rate (velocity). The right hand end tail also corresponds with the prediction. We can therefore also conclude that the 'cut' of the cyclone is determined by centrifugal separation, upon which the model is based. The fact that the measured curve is above theory indicates that the flow in and around the swirl element provides additional separation, for which the model does not account. Instead of providing a sharp 'cut', this additional separation mechanism seems to lower the distribution as a whole.

Despite the fact that the mist separation efficiency conformed to expectations, or even somewhat better, the performance with regard to big droplets (>200 µm) was inferior. This resulted in a low overall efficiency, 75% at the design load. The higher the gas velocity, the larger was the volume of large droplets measured in the flow leaving the cyclone. The reason is that the centrifugal force goes to zero at the stationary wall, which easily leads to re-entrainment. Since the RPS has a rotating collection wall, it does not suffer from this problem.

RPS

Many RPS devices have been designed and tested over the past 15 years[5-7], e.g. ash removal from the flue gas of combustion installations, air cleaning in domestic appliances, product recovery in the pharmaceutical and food industries, and oil/water separation.

Separation efficiencies have been assessed for a number of separation elements of different size (length, radius, channel, height, etc.) subject to different conditions (angular speed, flow rate, particulate matter, etc.)[7,12,13]. Particle collection efficiencies were determined by measuring distributions at the inlet and outlet using cascade impactors and laser particle counter techniques. For each case the value of d_{p50} according to equation (6) was calculated: d_{p50} varied from a value as small as 0.1 to 3 µm. The values of d_{p50} were subsequently used to generate separation efficiency distributions as a function of dimensionless particle diameter. Results are shown in Figure 10. For reasons of comparison the theoretical curve is shown as well. It is seen that the results of measurements are consistent with each other and compare sufficiently well with theory for design purposes.

Flow Stability

Although at first glance appearing to be simple and straightforward, the radial motion of phases and particles in a channel is a subtle and sensitive process. The smallest fractions aimed at being separated are those which move with a radial velocity that compares to the axial fluid velocity as the ratio of channel height to channel length, as implied by equation (6). In practical applications of the RPS this ratio is very small, typically <0.01. So the smallest separated fractions move with radial velocities which are only 1% of the axial fluid velocity. If secondary fluid flows occur in planes perpendicular to the axial channel axis which

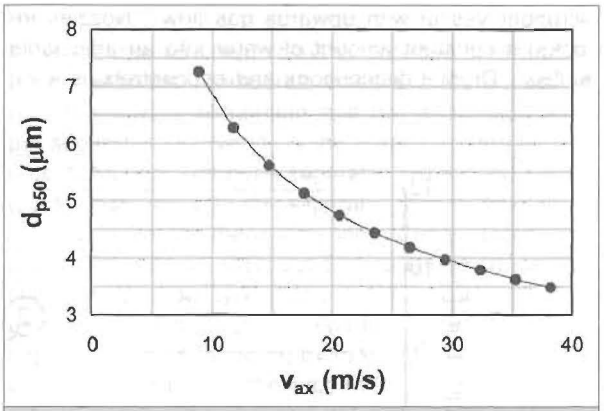

Figure 8: Axial cyclone d_{p50} as a function of mean axial velocity v_{ax}. Swirl ratio $S = v_t/v_{ax} = 1.2$ and $L/R = 5.6$.

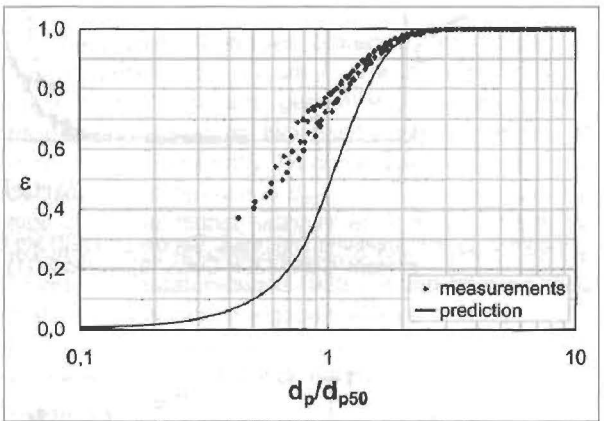

Figure 9: Measured efficiency ε as a function of the particle size d_p, made non-dimensionless with d_{p50}. Results below 3 µm were disregarded. Prediction is based on plug flow, and a Rankine vortex profile with core radius 0.8R.

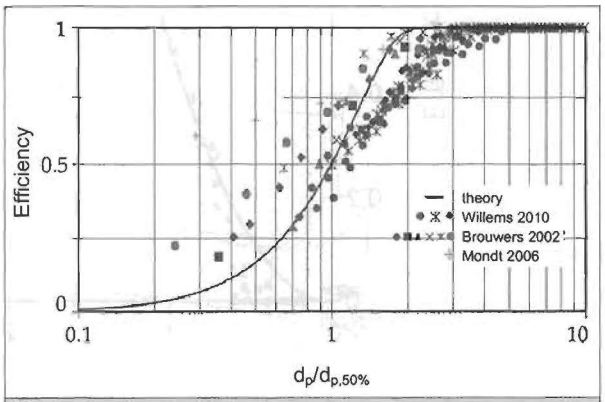

Figure 10: Efficiency of the RPS.

are only 1% in magnitude of the axial fluid velocity, the process of radial migration of the smallest separated fraction may already be disturbed.

Usually, the flow in the channels of the filter element is kept in the laminar regime to prevent capture of particles or droplets in turbulent eddies or swirls. In the case of large volume and/or high pressure applications the laminar flow condition may impose a too severe restriction on the design.

In most cases the Reynolds number is low enough for the flow and particle behaviour to be studied in detail by means of direct numerical simulation of the fluid flow and Lagrangian particle tracking[12,13]. The results of the fluid flow show that an axial vortex is present in the flow, caused by the rotation, but also that this vortex hardly influences the collection efficiency. However, turbulent velocity fluctuations have a negative influence on the collection efficiency, especially for larger particles (Figure 11). In order to meet design criteria in practice, the length of the RPS should be chosen to be about 20% larger than the laminar design criteria prescribed to obtain the same collection efficiency. The results confirm that when the rotational particle separator is used as a bulk separator and a strictly defined cutoff diameter is not required, the working range can be extended in the turbulent range to enhance the throughput within the same volume constraints. This is a major advantage in offshore applications where platform space and load capacity are at a premium and recent designs of the RPS for natural gas treatment[3,6] are operating in the turbulent regime.

Unwanted secondary flows can also occur in the case where symmetry axis of a channel makes an angle with respect to the rotation axis. For example, by fabrication inaccuracy the channels can be twisted around the symmetry axis of the filter element, or they can diverge or converge as their distance from the axis of the filter element increases (or decreases) in the axial direction. Coriolis forces will act on the fluid as soon as the fluid flow is non-parallel to the rotation axis[14]. Such forces lead to circulatory secondary flows in planes that are perpendicular to the axial channel axis of a kind similar to the circulatory flows in bends. For circular pipes it is possible to calculate these flows analytically as solutions of the Navier-Stokes obtained under certain limiting conditions that coincide with the conditions under which the RPS operates[16]. In practical design it implies that non-parallellity of the channels must be limited to specific values, to angles of inclination of a few degrees in typical cases.

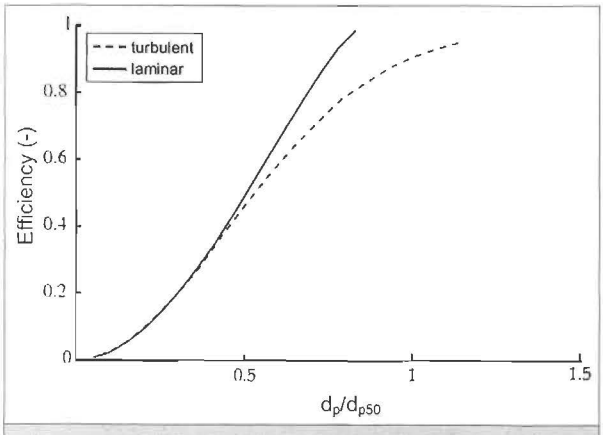

Figure 11: Efficiency of the RPS for laminar and turbulent flow.

Power Consumption

The power consumption of both the RPS and cyclone has been investigated in detail[1]. Energy consumption occurs mainly through the pressure drop that the fluid undergoes when flowing through the apparatus. One can assume that swirl induced at the entrance (and associated radial pressure buildup) is eventually lost: the irreversible pressure loss can be taken to be equal to $\rho_f v_t^2$. The total energy loss (E) can be calculated by integrating over all radial positions. For constant v_t and v_{ax} with respect to r, the result is $E = \rho_f v_t^2 Q$. Energy consumption per unit mass flow, $\varepsilon = E/(\rho_f Q)$, then amounts to $\varepsilon = v_t^2$.

The flow through the filter element channels of the RPS constitutes an extra pressure loss of $\Delta p_{ch} = \rho_f v_a x^2 f L l/(2d_c)$. The friction factor for laminar flow in a round channel is $f = 64\mu/(\rho v_{ax} d_c)$. Here we disregard the extra pressure losses due to entrance effects, as well as blockage of the channels, in practice these amount to <10% of the channel pressure drop. We have shown that as liquid builds up on the channel walls, shear stress exerted on the liquid is large enough to tear the liquid stream into large separable droplets downstream of the RPS[3]. We can then write for the specific energy consumption:

$$\varepsilon_{ch} = \frac{S64\mu L}{\rho_f d_c^2} v_t = O(1) v_t \qquad (10)$$

which in most cases can be neglected compared to the swirl term v_t^2. We can therefore conclude that the energy consumption of an RPS in the first order is comparable to a cyclone with similar swirl velocity.

Loading

For certain applications, filter cleaning involves removal of the filter element from the apparatus, which is followed by cleaning and reintroduction or by replacement. For most industrial applications, however, in-situ filter cleaning is preferred, without or with limited interruption of the filtering process.

For air-jet cleaning a nozzle is fitted on top of the RPS which can move radially from the inner to outer radius

of the filter element (Figure 12). Once the channels of the filter element become saturated with particulate material the jet starts to blow into the channels. This can occur during normal filter operation. The radial width of the nozzle compares in size with the height of the channels, i.e. a few millimetres. Due to filter rotation, a moment will occur when the channel has passed the column of air blown from the nozzle whence expansion waves start to develop from the top of the channel and result in intense cleaning of the channels[2]. It has been established that about 1 kg of fine particle material collected in the channels can be removed by injecting about 1 kg of compressed air at 6 bar.

As an alternative to air (or other gases), cleaning of the filter element can be accomplished by periodically injecting water (or other liquids). In practice it has been established that (hot) water at pressures of 50 to 100 bar can be injected using the same nozzle as the one used for air. It offers the possibility of cleaning the filter from time to time very thoroughly with (hot) water, in addition to a regular air cleaning. It is particularly interesting for applications where high standards of hygiene apply.

A third method for removing particle material from the channels of the filter element is to continuously add liquid. This can occur by dispersing a spray of fine liquid particles that are centrifuged towards the outer walls of the channels of the filter element. Here they form a liquid film which moves downwards and carries away the other (solid) particles. The wet version of the RPS appears to be an attractive alternative to existing wet scrubbers that are often employed in the chemical and process industries. In contrast to wet scrubbers, in the RPS water is not injected to separate particles, but only to transport the particle material being centrifuged towards the walls. This results in much lower (by up to two orders of magnitude) amounts of washing liquids[9].

In liquid applications a film builds up along the walls of the channels. The speed at which the film can be drained determines the maximum liquid load. Both theory and experiments[3] show that liquid loads up to 50% by mass can be drained effectively.

APPLICATIONS

Phase separation in centrifugal fields using the RPS has found its way, or is on its way, to the market in various areas of application (Figure 13). A multinational electronic consumer goods company has adopted the principle in an air cleaner. The device, which is sold worldwide, serves to remove the airborne particles that can cause respiratory allergic reactions to men in houses and offices.

Another application concerns the collection of powders and particles from gases in food and pharmaceutical processes. A specific advantage in this area is the possibility of fabricating the entire apparatus from stainless steel, and of meeting the stringent conditions for hygiene and cleaning. A design was shown in Figure 11. The rotating element has been integrated in a

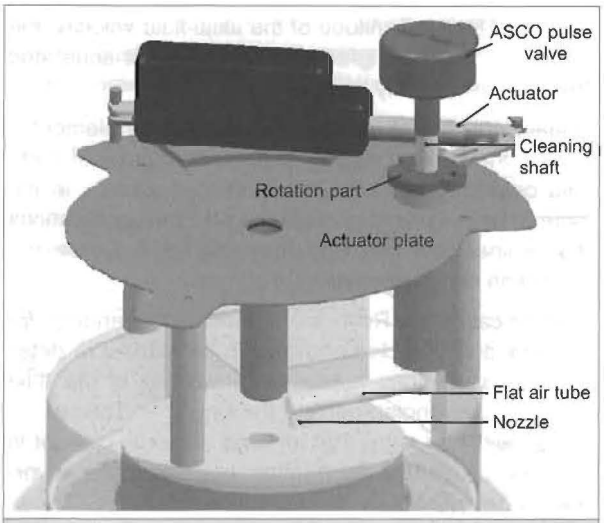

Figure 12: Jet cleaning system of an RPS.

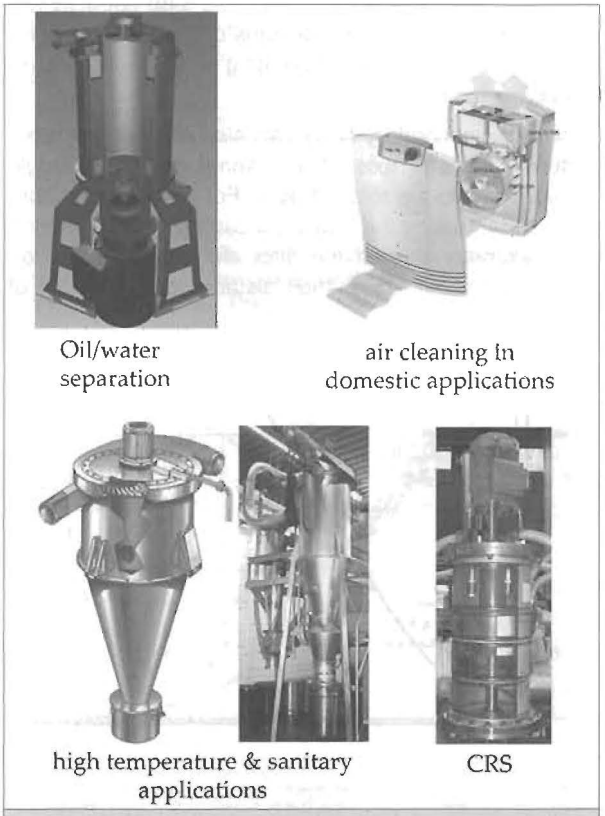

Figure 13: Application examples of the RPS.

cyclone. The cyclone acts as a pre-separator in which the gas is filtered from coarse particle material prior to entrance into the separation element. The cyclone also serves as a pre-swirler within which the gas is brought in rotation before entering the rotating separation element.

An impeller is fitted to the downstream side of the filter element such that the gas is brought to the desired pressure. Doing so avoids the necessity of installing a separate fan which compensates for the pressure loss incurred in the separation device. Moreover, the overpressure in the exit chamber ensures that only clean air flows through the gap between the rotating filter element and the housing from the exit chamber to the inlet chamber/cyclone, instead of unfiltered air moving *vice versa*. Air nozzles are placed on top of the device so that periodically the material collected in the channels is blown towards the cyclone where it is collected in the cyclone outlet. Blowing occurs during normal operation of the filtering process, without stopping flow and rotation.

The RPS device can be made heat resistant in order to allow operating temperatures up to 500°C. This has facilitated applications for filtering hot gases of small and medium sized coal and wood combustion and gasification installations. Another feature is the ability to simultaneously separate solid and liquid particle materials which has led to the development of units suited to the filtering of polluted and misty intake air of land-based gas turbines for power generation.

In a more recent development the filter element is combined with a multistage pump to coalesce micron-sized oil droplets to over 30 times their original size[10]. Together with the water, the large droplets leave the coalescing pump to be separated in a conventional separator placed downstream.

Condensed Rotational Separation: A Compact and Energy Efficient Process for Gas-Gas Separation

The RPS facilitates various kinds of innovations in the process industry, an example is condensed rotational separation[8]. In this process components of a gas-gas mixture are condensed by the fast reduction of temperature and pressure. The resulting mist of micron-sized droplets is removed by the RPS. Applications foreseen are: upgrading of contaminated sour gas fields[8], removal of CO_2 from the flue gases of coal fired power stations[16] and separation of heavy fractions from natural gas. The core of all these applications is the RPS, designed as a compact mist and aerosol catcher.

RPS Gas Scrubber

The introduction of the RPS as a gas scrubber in large volume applications[6] presented a number of new design issues, the most important being the behaviour under high pressure and the ability to cope with large liquid loads. As it is known that centrifugal separation is a process that is sensitive to design details that are easily overlooked in CFD simulations, a visually accessible industrial scale prototype has been built before taking the step to a field test. The prototype was connected to an atmospheric test rig with water and air as working fluids. The test setup approximately models a 24 m^3/s (80 MMscf/d) equivalent installation on a natural gas well. The design is suited to large liquid loads and is depicted schematically in Figure 15.

Gas containing a mist of droplets enters the unit via a tangential inlet. First, coarse droplets (larger than 10 µm) are separated in the pre-separator section. The pre-separator acts as a cyclone and collects the droplets in a stationary volute. This liquid leaves via a tangentially connected exit. The gas stream, containing the remaining mist of mainly micron-sized droplets, enters the rotating element. In the design the rotating element can be driven by the impulse of the rotating flow. An external drive can optionally be added to be able to control the rotating speed independent of the incoming flow. While travelling in the axial direction through the rotating channels, the droplets are driven to the channel walls by centrifugal force. On the walls the mist droplets coagulate into a thin film and the rotating element thus acts as a droplet coalescer. For optimal film behaviour and minimal pressure drop the

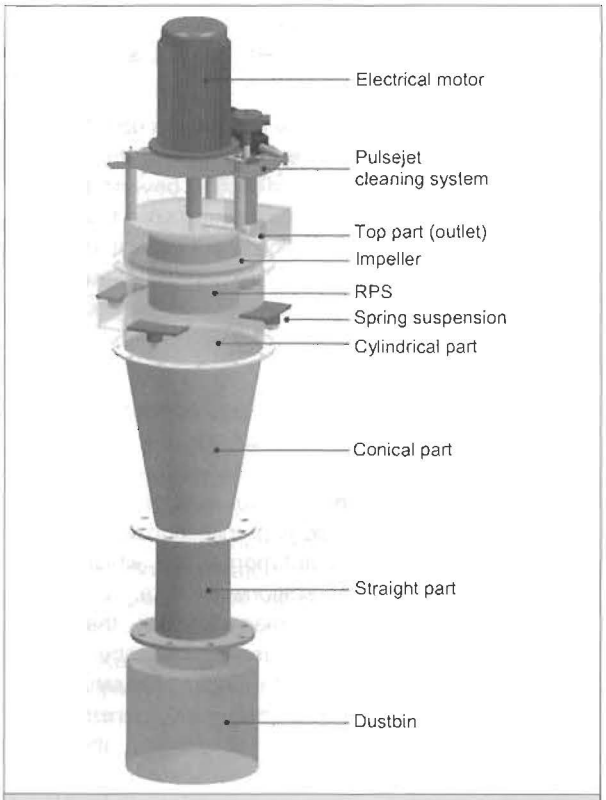

Figure 14: RPS integrated with a cyclone and fan.

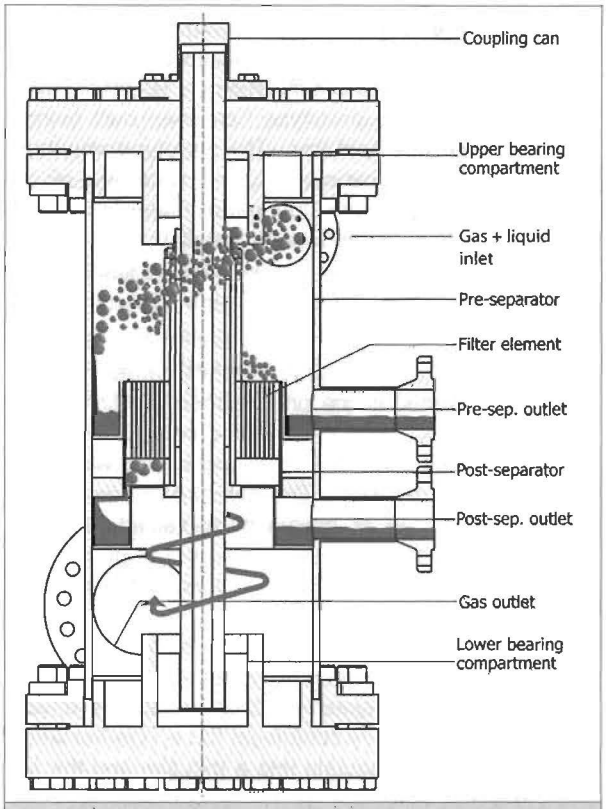

Figure 15: High volume RPS mist catcher design.

flow direction through the element is downward. Due to gravitational and shear forces, the film is forced out of the channels.

At the end of the channels the film breaks up into droplets of typically 50 µm. The outer wall of the rotating element extends in the axial direction beyond the end of the channels which ensures that the solid body rotation of the gas stream leaving the element is maintained. Droplets that break off at the end of the channels are centrifugally separated from the gas in this rotating field, and collected in a film on the rotating outer wall.

Downstream of the element the post-separator section is entered, where the liquid is actually separated from the gas stream. The liquid film leaves the gas stream at the end of the extended outer wall of the rotating element towards a non-rotating collection volute. The liquid still contains significant momentum, which drives a standing film within the stationary volute. Via a tangentially connected large diameter exit the liquid leaves towards a collection vessel. The inner wall of the collection volute keeps the liquid separated from the product gas flow. This wall prevents re-entrainment of liquid due to splashing in the post-separator.

The RPS is designed to minimize any complexities involving rotation and this is achieved by containing all rotating parts, including bearings, in a pressure resistant pipe. Hence, there are no rotating shafts that pierce through the wall which eliminates the need for rotating seals. If an external drive is needed then this happens through a magnetic coupling. Furthermore, the rotating element is simple and straightforward in terms of design, thereby leading to low mechanical stresses. It is easy to design for a continuous lifetime of ten years or longer.

After assessing that the RPS performed to expectations regarding separation efficiency and liquid removal[11] the test rig was modified to simulate the behaviour at higher Reynolds numbers. It is known that non-rotating pipe flow becomes turbulent due to finite amplitude disturbances for bulk Reynolds numbers, Re > 2000. However, sufficient rotation causes the flow to already become unstable against infinitesimal disturbances at Re = 83[15]. Therefore, rotating pipe flow is characterized by two Reynolds numbers: the usual bulk Reynolds number, $Re = v_{ax} d_c \rho_l / \mu$, and an additional rotation Reynolds number, $RR = \Omega d_c^2 \rho_l / 4\mu$ which comprises the rotation rate Ω (rad/s), but is independent of the distance to the rotation axis. It should be realized that, although these conditions are sufficient for the onset of instabilities, they need not correspond to the transition to turbulence.

An important implication of applying the RPS under pressure is a high gas density, which accompanies the large Reynolds numbers. Since our laboratory test setup operates with air at atmospheric pressure, we used an extra large channel diameter to achieve a higher Reynolds number. Since the channel length to diameter ratio was kept constant, the test unit had to be lengthened as well. Figure 16 shows a measurement result that was obtained using the method explained earlier. It can be concluded that sufficient separation is achieved, also in the unstable/turbulent regime. Compared to laminar flow, d_{p50} does not change, while the right hand side of the curve drops only slightly, conform DNS simulations. We can now safely disregard the earlier restriction of purely laminar flow.

Often the performance of a gas scrubber is presented in the form of a sizing or load factor, K, as used in the Sounders-Brown equation. The required gas scrubber area (footprint) can than be calculated from

$$A = \frac{Q_A}{K} = \sqrt{\frac{\rho_l}{\rho_l - \rho_g}} \qquad (11)$$

The load factor, K, is a direct measure for the required footprint of the installation and has the unit of velocity. In Figure 17 we have compared the best practice of scrubbers with that of a RPS. Only under atmospheric

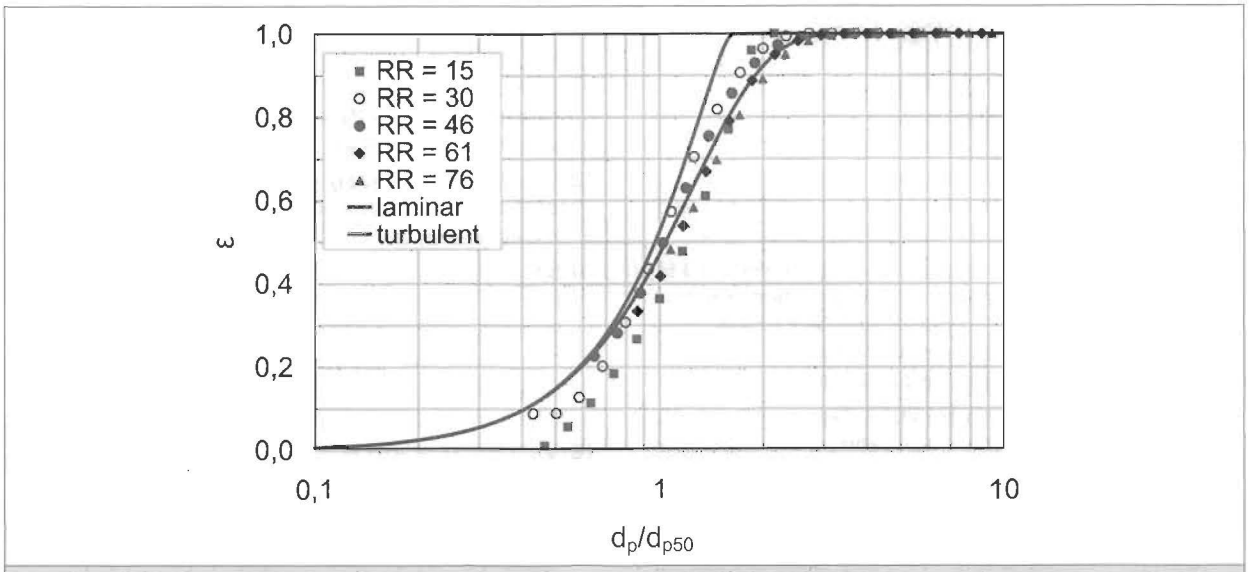

Figure 16: Efficiency of the RPS with unstable flow in the rotating channels (Re = 1070).

pressure and a d_{p50} of 3 μm is the size of a cyclone deck comparable to that of a RPS. Otherwise the RPS is significantly smaller and capable of separating particles in the sub-micron range. Thus, application of the RPS is particularly advantageous when working at elevated pressures and large flows as is the case in the process of condensed rotational separation.

CONCLUDING REMARKS

The main features of the RPS as a new device for separating micron sized particles or droplets from carrier fluids have been presented. Performance indicators such as the size of particles separated, energy consumption per unit throughflow and size of the unit compare favourably with conventional methods based on vane separators and cyclones. The RPS facilitates various innovations in the process industries. An example is the compact and energy efficient process of condensed rotational separation.

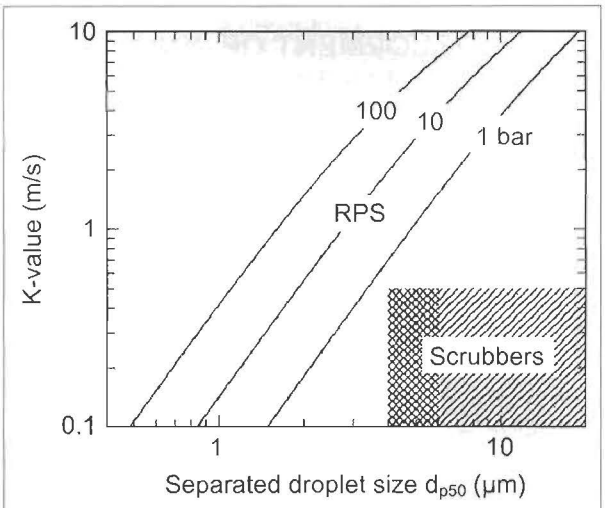

Figure 17: *K*-values for the RPS and scrubbers. Crosshatch pattern indicates best practice using cyclone decks.

ACKNOWLEDGMENT

The authors wish to thank Romico Hold for access to proprietary knowledge regarding the RPS and related processes.

REFERENCES

1. van Wissen R.J.E., Brouwers J.J.H. and Golombok M., 2007. In-line centrifugal separation of dispersed phases, *AIChE J*, **53**(2), 374-380.
2. Brouwers J.J.H., 1997. Particle collection efficiency of the rotational particle separator, *Pow. Technol.*, **92**, 99-89.
3. Willems G.P., 2009. *Condensed Rotational Cleaning of Natural Gas*, PhD Thesis, Eindhoven University of Technology.
4. Houghton H.G. and Radford W.H., 1939. Measurements on eliminators and the development of a new type for use at high gas velocities, *Trans American Chemical Engineers*, **35**, 427–433.
5. van Kemenade H.P., Mondt E., Hendriks A.J.A.M. and Verbeek P.H.J., 2003. Liquid-phase separation with the rotational particle separator, *Chem. Eng. Techn.*, **26**(11), 1176-1183.
6. Mondt E., van Kemenade H.P. and Schook R., 2006. Operating performance of a naturally driven

rotational particle separator, *Chem. Eng. Techn.*, **29**(3), 375-383.

7. Brouwers J.J.H., 2002. Phase separation in centrifugal fields with emphasis on the rotational separator, *Exp. Therm. Fluid Sci.*, **26**, 325-334.
8. van Kemenade H.P., Brouwers J.J.H. and Benthum R.J., 2011. Condensed rotational separation, *AFS Annual Conference*, 10-12 May, Louisville, USA.
9. Mondt E., van Kemenade H.P., Brouwers J.J.H. and Bramer E.A., 2004. Rotating sorbent reactor, *3rd International Symposium on Two Phase Flow Modelling and Experimentation*, Eds: G.P. Celata, P. Di Marco, A. Mariani and R.K. Shah, Pisa, Italy.
10. Liebrand H. and Wals E., 2011. New technology to improve the performance of produced water separation systems, *9th Produced Water Workshop*, Aberdeen, 18-19 May.
11. Willems G.P., Kroes J.P., Golombok M., van Esch B.P.M., van Kemenade H.P., and Brouwers J.J.H., 2010. Performance of a novel rotating gas-liquid separator, *J. Fluids Eng.*, **32**(3), 031301.
12. Kuerten J.G.M., van Esch B.P.M., van Kemenade H.P. and Brouwers J.J.H., 2007. The effect of turbulence on the efficiency of the rotational phase separator, *Int. J. Heat Fluid Flow*, **28**, 630-637.
13. van Esch B.P.M. and Kuerten J.G.M., 2008. Direct numerical simulation of the motion of particles in rotating pipe flow, *J. Turbulence*, **9**(4), 1-17.
14. Brouwers J.J.H., 1995. Secondary flows and particle centrifugation in slightly tilted rotating pipes, *Applied Scientific Research*, **55**, 95-105.
15. Mackrodt P.A., 1976. Stability of Hagen-Poiseuille flow with superimposed rigid rotation, *J. Fluid Mech*, **73**(1), 153-164.
16. Van Kemenade H.P., van Benthum R.J., Brouwers J.J.H. and Golombok M., 2011. Condensed rotational separation of CO_2, *The Clearwater Clean Coal Conference*, 5-9 June, Clearwater, Florida, USA.

DEVELOPMENT OF INNOVATIVE FIBRE MATERIALS FOR TECHNICAL APPLICATIONS – FINE POLYVINYLIDENE FLUORIDE FILAMENTS AND FABRICS

Stephan Walter[1] (stephan.walter@ita.rwth-aachen.de), Wilhelm Steinmann[1], Gunnar Seide[1], Thomas Gries[1] and Georg Roth[2]

[1]*Institut für Textiltechnik, RWTH Aachen University, Aachen, Germany.*

[2]*Institut für Kristallographie, RWTH Aachen University, Aachen, Germany.*

Development of new materials and processes for technical applications usually requires extensive interdisciplinary cooperation. It is seldom that innovative and sophisticated materials evolve solely from one technical or scientific discipline's efforts. In this paper the development of fine melt spun polyvinylidene fluoride multifilament yarns, the processing, fabric production and property investigation are presented. It outlines what it takes to exceed the state-of-the-art for existing fibre materials and their applications. The steps of material selection, experimental evaluation of a process window for melt spinning PVDF, yarn processing and fabric formation are reported in detail. Furthermore, a model for the crystalline structure formation during melt spinning and drawing PVDF fibres is presented.

INTRODUCTION

Polyvinylidene fluoride (PVDF) is a semi-crystalline polymer which has been given growing attention as a fibre polymer in the past few years[1-9]. This attention is caused by the interesting and unique property profile of PVDF. It is a semi-fluorinated polymer which is processed into injection moulded parts, films, textiles and coatings. It is chemically and bio-chemically very stable and resists most acids and bases[10]. It is suitable for medical applications as it is bio-chemically inert and NDA certified. At the Institut für Textiltechnik der RWTH Aachen University (ITA), Germany, extensive research has been, and is being, carried out on textile implants made from PVDF fibres[8].

PVDF exhibits multiple crystal phases. The linear polymer chain consists of repeating monomer units -[CF2-CH2]- with alternating hydrogen and fluorine side groups. The molecular structure results in an excellent chemical resistance. Furthermore, the electronegative fluorine atoms cause a dipole moment perpendicular to the polymer chain, which is responsible for the ferroelectric, pyroelectric and piezoelectric properties of PVDF. The occurrence of the special electric properties depends on the formation of a polar crystal phase, the so called β-phase. The α-phase (form I) develops in the melt spinning process[11], whereas the β-phase (form II) converts from the α-phase in the drawing process[12]. The polar character of the molecular struc-